Materials Research. 2023; 26:e20230219
DOI: https://doi.org/10.1590/1980-5373-MR-2023-0219

22MnB5 Performance as Surface Protection Mask Under Harsh Forging Conditions and its Wear Insight

Luana De Lucca de Costa[a]*, Alberto Moreira Guerreiro Brito[a], André Rosiak[a], Lirio Schaeffer[a]

[a]Universidade Federal do Rio Grande do Sul (UFRGS), Departamento de Metalurgia, Porto Alegre, RS, Brasil.

Received: April 29, 2023; Revised: August 08, 2023; Accepted: September 01, 2023

Herein, the applicability and performance of 22MnB5 steel sheets as protective masks over hot forging dies has been analyzed. Two masks were obtained following two different approaches; by heat treatment of flat sheets in cooling conditions similar to the process of hot stamping and hot stamping on the axial geometry of a cylindrical part. In both processes the sheets were austenitized at 1100° C for 7 min and to obtain bainite microstructure, they were maintained at temperatures higher than 700°C. The flat and axial masks have been subjected to 100 forging cycles for each geometry and positioned on the lower surface of hot forging dies. Surface integrity has been analyzed from microhardness profiles, roughness tests, thickness measurements, optical and electron microscopy. Wear mechanisms have been observed in both masks which was more expressive in the axial mask. Abrasive wear and plastic deformation have been actively observed in both masks; however, they have shown firmness for application as masks.

Keywords: *Protective mask, Tool live, 22MnB5, hot stamping.*

1. Introduction

Economically, forged products are attractive due to their high strength when exposed to the mechanical stresses, homogeneous microstructure and a greater ease by which the forged parts can be post-processed by the automated methods[1-3]. Technical researches have shown the wear is the predominant degradation mechanism in hot forging tools which is the result of a complex interaction of variables that constitute the tribosystem of hot forging process[4-6]. The wear and other failure mechanisms start from the surface of the dies which contributed to the development of surface coatings techniques. The main focus of these techniques is to improve the tools life due to the modification of surface properties. Since their longer use necessitates the repairs or replacements; therefore, surface treatments such as coatings, nitriding, and welding overlays are usually applied to protect them which are expensive[7-10]. In addition, the tools replacement causes a long interruption time during production. Rosenstock et al.[9] have investigated a new concept named the protective sheet metal die cover to protect the die surface to reduce the costs and production interruption time. The numerical simulation conducted by Rosenstock et al.[9] and Hawryluk[8] have highlighted the use protective masks on the forging dies that reduce the thermal and mechanical loads; thereby, the die working life can be extended. When compared to the conventional surface treatment methods, the masks are advantageous as without exchanging the forging dies they can be applied and their replacement is easy which helps decreasing the interruption time. Furthermore, these studies did not evaluate the ability of die covers to withstand the forming conditions occurring under a significant number of cycles. Earlier in the literature, the boron alloys particularly 22MnB5 have shown promising mechanical resistances[11,12]. Yu et al.[10] have tested 22MnB5 as mask manufactured by deep drawing and later subjected to 40 forging cycles. Hot stamping is an emerging technology to increase the 22MnB5 steel grade strength extensively used in automobile industry[13,14]. It would be interesting to use 22MnB5 steel grade as mask produced by hot stamping and also attempts are necessary to expose it to intensive forging cycles that can help understanding further possibilities to its industrial applications.

In this work, 22MnB5 has been tested as flat and axial masks after 100 forging cycles over hot forging dies. Detailed surface, mechanical and microstructural properties of the material have been investigated by a wide range of characterization techniques.

2. Materials and Methods

Initial sheets of 110 mm in diameter and 1.3 mm in thickness of 22MnB5 were used to manufacture masks. Two methods to obtain these masks were performed: 1) The initial sheets were heated between the flat dies under the predetermined conditions established in the literature for hot stamping[14,15]; 2) The initial sheets were hot stamped, without the use of refrigerated dies in a cylindrical form.

In the heat treatment process, the sheet was austenitized, transferred, and positioned on flat dies at room temperature to obtain the flat mask (Figure 1). When the set of flat dies is closed, the phase transformation occurs.

Table 1 lists the parameters of the heat treatment process to obtain the flat mask.

*e-mail: luanadldcosta@gmail.com

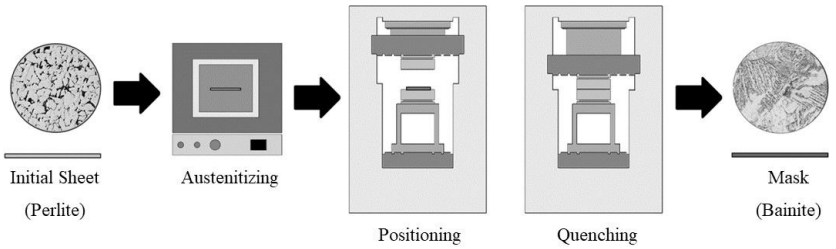

Figure 1. Heat treatment process to obtain the flat mask.

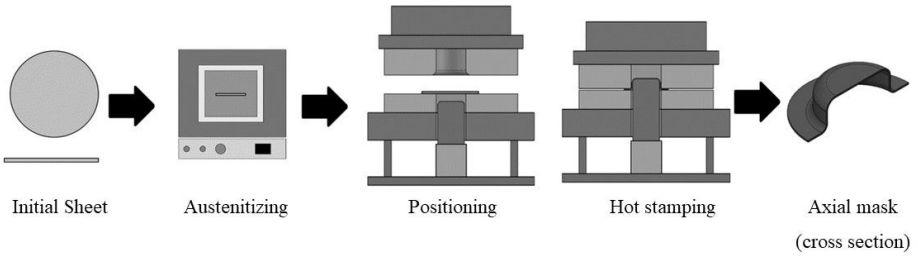

Figure 2. Hot stamping process to obtain the axial mask.

Table 1. List of parameters of the heat treatment process.

Heat treatment process parameters	
Heating	Electric furnace (Chamber)
Austeniting time	7 min
Austeniting temperature	1100°C
Press (no acting)	Hydraulic press (single acting) (FKL)
Press speed	9 mm/s
Dies temperature	Room temperature

Table 2. List of parameters for the hot stamping process.

Parameters of the hot stamping process	
Heating	Electric furnace (Chamber)
Press	Double-acting hydraulic press (DanPres)
Normal force	200 kN
Press speed	Varieble
Lubrification	FORGE EASE 956BR
Initial sheet temperature	1100°C
Tools temperature	Room temperature

Figure 2 shows schematically the process of hot stamping of axial masks. The sheets were heated and positioned in the center of the stamping die. After positioning, the die is closed and the punch is activated.

Table 2 lists the parameters of the hot stamping process to obtain the axial mask.

The flat dies and the hydraulic press (FKL) used in the heat treatment process were used in forging process. The material of the forging dies (H13) was selected based on its metallurgical characteristics such as an exceptional hot hardness and abrasion resistance. The masks were positioned in the lower dies. In both processes, cylindrical billets of 35 mm in diameter, height of 70 mm, and volume of 67340 mm^3 of AISI 1045 were forged. Figure 3 shows the 3D design of the dies used for both forgings with the masks positioned for forging processes.

Tables 3 and 4 display the parameters of the open and closed die forging processes.

The masks surface images were acquired using a Stereomicroscope with LED and HD camera, Leica brand, model EZ4 HD (4:1 scale). The thickness variation was measured using a digital micrometer Mitutoyo, scale 0-25 mm, with a resolution of 0.001 mm.

Profiling tests were performed on the surfaces of the masks using XP-2 profilometer from Ambios Technology coupled with the True Surf® software. To evaluate the microstructure, conventional metallography techniques were used in the cross section of the masks using Olympus Gx51optical microscope, samples parallel to the compression direction from cross section of the masks and from the cross section of inicial sheets (as-received microstructure) were prepared following standard procedures[16] and etched by immersion in a Nital 2% solution for 10 s. Scanning electron microscopy (SEM) was used to analyze the surface condition of the masks in a cross section view by Zeiss EVO MA 10, the parameters used to acquisition are shown in the images. The microhardness profile was acquired in Insize Hardness Tester ISH-TDV1000 microdurometer according to ASTM standard E384, the measurements were conducted on the cross-sectional area of the mask, 0.5 kg, at 1.25 mm intervals. The chemical compositions of steels were obtained by glow discharge optical emission spectroscopy (GDOES). The removal of the oxidized layer was carried out through blasting with glass microspheres with a hardness ranging

Table 3. List of parameters of the open die forging process.

Parameters of the open die forging process	
Heating	Electric furnace (Chamber)
Press	Hydraulic press (single acting) (FKL)
Normal force	400 kN
Press speed	9 mm/s
Billet height reduction	35 mm
Mask and upper die lubrication	FORGE EASE 956BR
Lubrication between the mask and the lower die	-
Initial temperature of the lower die	280°C
Initial mask temperature	280ºC
Initial temperature of the upper die	Room temperature
Billet initial temperature	1100°C

Table 4. List of parameters of the closed die forging process.

Parameters of the closed die forging process	
Heating	Electric furnace (Chamber)
Press	Hydraulic press (single acting) (FKL)
Normal force	400 kN
Press speed	9 mm/s
Mask and upper die lubrication	FORGE EASE 956BR
Lubrication between the mask and the lower die	-
Initial temperature of the lower die	280°C
Initial mask temperature	280ºC
Initial temperature of the upper die	Room temperature
Billet initial temperature	1100°C

between 5 and 7 MOHS and an average size of 150 µm. This method was chosen for its low abrasiveness, attributed to the spherical shape combined with the hardness and density of glass, allowing for the removal of contaminations.

3. Results and Discussion

The chemical composition of the materials used to manufacture the initial samples, billets for forging processes, and the tools are listed in Table 5.

The optical micrograph shows that in the initial condition, 22MnB5 has a ferritic microstructure with a homogeneous distribution of perlite, 184 HV; typical to low carbon steels. The micrograph is shown in Figure 4.

The bainitic microstructure is formed after heat treatment and hot stamping. The micrographs are shown in Figure 5.

At the end of the 100 forging cycle over the flat mask, the surface topography is shown in Figure 6. For the analysis, the mask was divided into three regions (Figure 6a): Region 1 is the central region that remains in contact with the forging billet during the entire forging cycles; region 2 corresponds to the area that is formed due deviation of billet from the central position where the billet marks are clearly visible and region 3 does not come into contact with the billet during the forging (Figure 6b).

In Figure 6a, it is possible to identify deformation marks caused by the billets. Region 3 shows marks of oxidation from the heat treatment and which could not be removed by the glass blasting process to which the mask was subjected after treatment. Figure 6b shows region 2 with 20x magnification, where the deformation marks of the billets on the mask are clearly identifiable in this magnification.

The initial average thickness of regions 1 and 2 is 1.28 mm and region 3 it is 1.33mm. After 100 forging cycles,

Table 5. Result of chemical analysis (w.t.%)

Material	C	Mn	P	S	Si	Cr	Mo	V	B	Fe
22MnB5	0.23	1.24	0.021	0.002	0.21	0.19	-	0.004	0.002	
AISI 1045 101045	0.42	0.72	0.020	0.041	-	-	-	-	-	
H13	0.37	0.32	0.018	0.002	1.12	5.30	1.16	1.00	-	

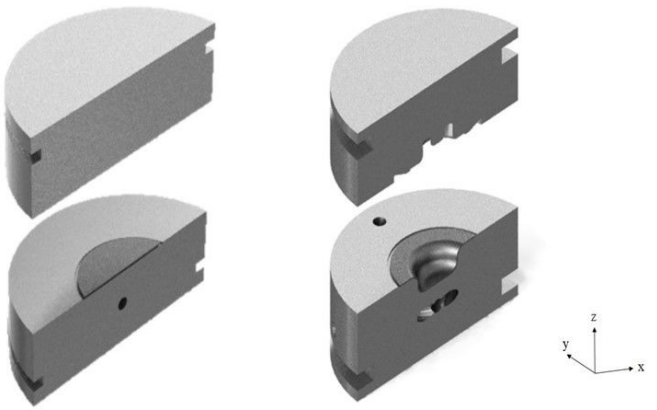

Figure 3. 3D cross section design of the dies for forging in open and closed die with the positioning of the masks.

thicknesses of regions 1 and 2 are 1.23 mm and 1.25 mm which show the deformations decreased the mask thickness.

The results of the roughness tests indicated the gradual removal of the material and the reduction of surface quality.

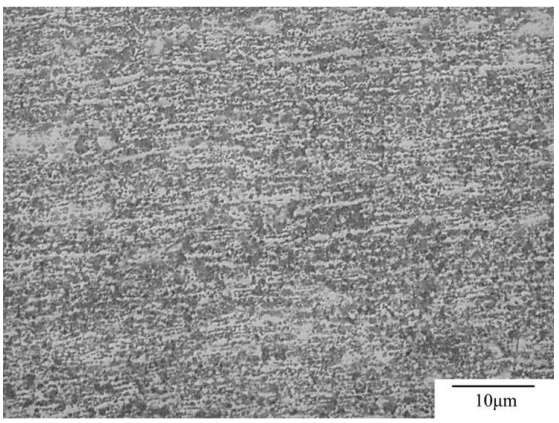

Figure 4. Optical micrograph of the initial condition in the longitudinal direction. Nital 2%.

The average roughness values (Ra) remained unchanged in region 3; being 0.28 µm initially and 0.30 µm after forging, in region 2 the value is 0.59 µm and in region 1 it is 0.76 µm.

The micrograph shown in Figure 7 indicates the microstructure remains morphologically bainitic in region 1 of the mask after the forging cycles. Although the microstructure continues to present bainitic morphology when compared to the values of the initial and final microhardness profiles, the softening in this region is noteworthy. The initial mask hardness values varied between 358 HV and 460HV and the average value was 416HV. These values were reduced to 250 and 390HV, with an average value of 268 HV. This softening indicates that the bainite temper has been occurred.

In region 2 there is a significant variation in microhardness values, starting with values of 300HV and ending with 370HV which closed to those values founded in region 3. As it is an intermediate region, it shows that softening proceeds from region 1 to region 3; thereby, the region 3 presents the highest microhardness which was uncontacted with the billet, 426HV.

The initial surface of the flat mask with and without forging cycles are shown in Figure 8; it is possible to observe signs of material displacement and cracks in Figure 8b.

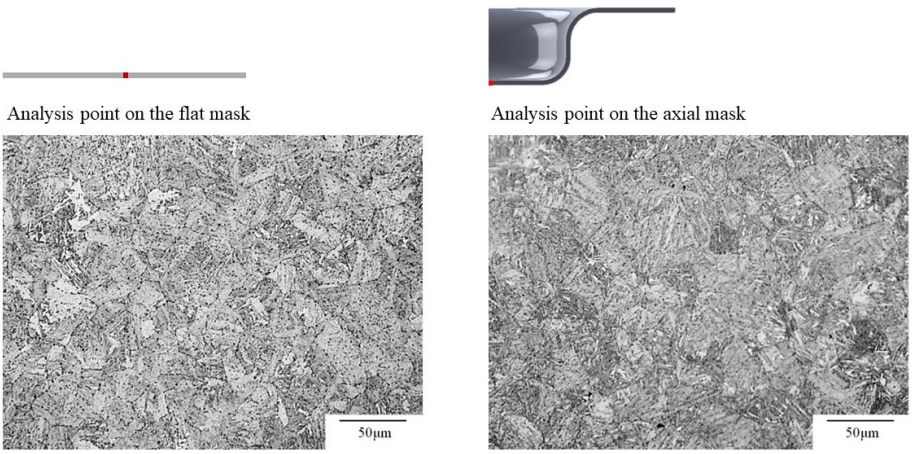

Figure 5. Optical micrographs of the points indicated on the flat mask (a) and axial mask (b). Nital 2%.

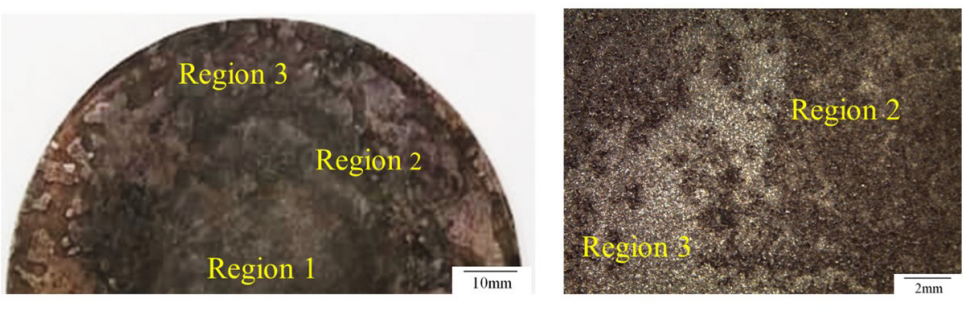

Figure 6. Flat mask with identification of the 3 different regions. (a) Sectional view showing the 3 regions and (b) Region 2 highlighted for 20x magnification.

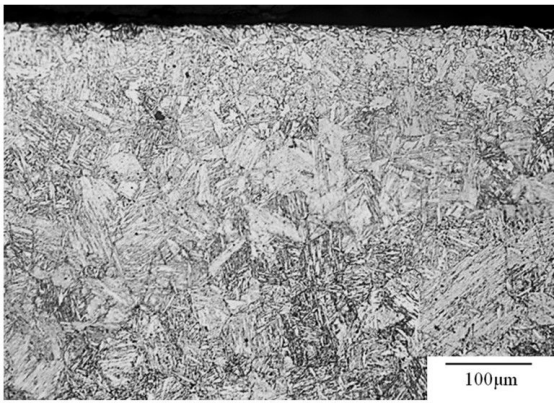

Figure 7. Optical micrograph taken from the middle of the region 1 of the flat mask after 100 forging cycles. Nital 2%.

As the number of forgings increases, the mask's contact with the oxides formed by heating the billet increases, and the abrasive wear and plastic deformation progresses[11]. In the image, it is possible to observe the superficial cracking that will cause the removal of part of the material on the surface.

The axial mask after 100 forging cycles is shown in Figure 9. The mask flange presents a change in shape attributed to the fact that the forging force is applied only until the end of the flash gutter and there is no restriction on the external movement of the flange; thereby, the deformation occurs due to press-flexion[15].

Figure 10 shows the mask surface subjected to 100 forging cycles with 20x magnification. In images a and b, it is possible to observe the surface degradation by oxidation and abrasion (a). In Figure 10a the wear is more expressive and originated by abrasion between the mask and the die. It is important

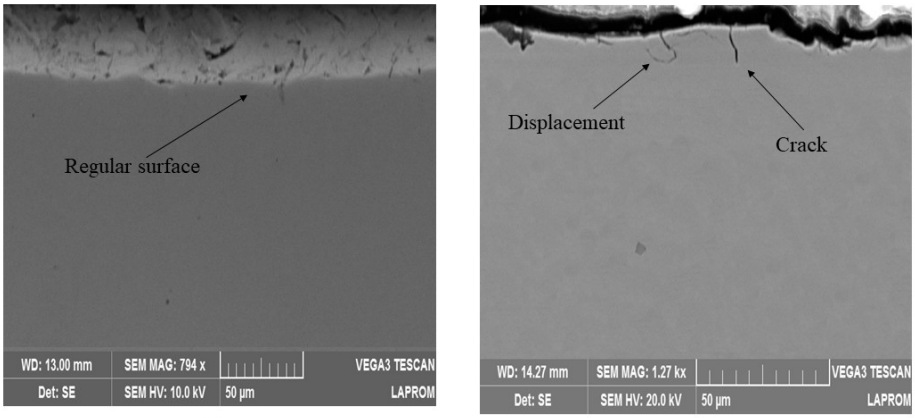

(a) (b)

Figure 8. Micrographs obtained by electron microscopy (SEM) of the surfaces of the flat mask (region 1): (a) Initial condition and (b) after 100 forging cycles.

Figure 9. Axial mask after the 100 forging cycle.

to note that no lubricant was used between the mask and the die, which justifies the expressive surface degradation.

In the lower external radius it is possible to observe the beginning of the removal of material on the surface of the mask that was in contact with the die during the forging process, Figure 10c. The flash land region has well-defined grooves in the flow direction of the forged material and there are also removal marks, as shown in Figure 10d. These were the failure mechanisms and the types of wear that could be observed up to the magnification of 20x.

Figure 11 shows the axial mask used in the 100 forging cycle with the thickness measurement points (a) and the thickness variation (b).

In the center, the initial thickness of mask is 1.19 mm and after 100 cycles there has been a reduction to 1.12 mm. The values increase at the beginning and decrease at the end of the r_2 region in the initial mask and after the forging process. The maximum value in the initial condition is 1.3 mm and the minimum value is 1.2 mm in r_2. After the 100 forging cycles, the maximum thickness reduction was 1.11 mm.

In the region of the mask wall, the initial thickness is 1.2 and has been a reduction to 1.1 mm after 100 cycles. In r_1 there is an increase in thickness at the center of the radius, the initial thickness increases to 1.3 mm and in the mask of the 100 forging cycle decrease to 1.29 mm. The greatest thickness reduction occurs in the first measurement, being initially 1.22 and 1.08mm after forging cycles.

Flash gutter and flange region demonstrate a hardly deformation starting in final of flash land region (Figure 9), wherever the thickness in these regions not shown an expressive reduction, it can be seen clearly in Figure 11 (points 11-16).

The results of the roughness tests indicate the gradual removal of the material and the reduction of surface quality after the forging cycles at all points studied in the axial mask, as indicated by the roughness Ra and Rz. Four different points were analyzed: inner center (C_1) and outer center (C_2), these points are shown in Figure 10, r_1 and r_2. In the initial mask, the Ra is 2.11µm, 4.08µm, 5.56µm, and 4.30µm, respectively. For Rz, the results are: 15.17µm, 28.01µm, 29.62µm and 25.57µm, with the highest values measured on the outside of the mask, C_2 and r_2.

The C_2 has the highest values in the studied profiles with Ra of 14.08µm and Rz of 41.88µm. Considering that Rz is the average distance between the 5 highest peaks and the 5 deepest valleys, within a measured length (ISO 4287), and comparing this value to the images shown in Figure 10, it is possible to observe the surface irregularity of these regions.

Comparing C_1 to C_2, C_1 has significantly lower values. The Ra for the is 11.42µm and Rz is 33.71µm. This is

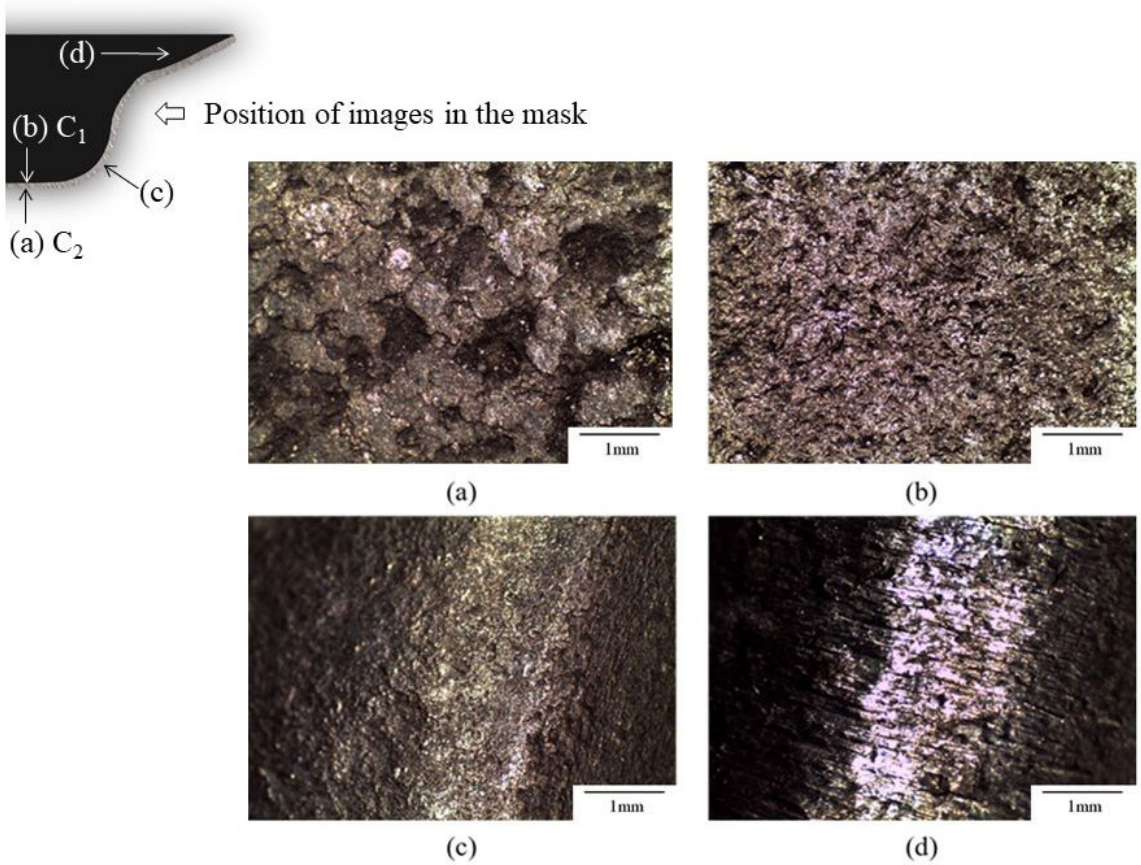

Figure 10. Metallic mask surfaces after 100 forging cycles, with positions indicated in the schematic representation: (a) Inner center (C1), (b) Outer center (C2), (c) External radius and (d) Inner flash land. Magnification 20x.

attributed to the use of lubricant only between the mask and billet, and the upper surface integrity can also be seen in the images of C_1 and C_2 in Figure 10.

The r_1 did not show significant oscillations in the Ra. In initial condition Ra was 5.56µm and after the forging is 8.95µm. This condition is the change in Rz, wherein the initial condition it is 29.62µm and 42,22µm after forging cycles. In this region, during the forging process, the filling of the cavity of the die is complete, and the material flow towards the flash gutter, then, the force acting on the process increases, and degradation in that region is accentuated.

In the region of r_2, Ra and Rz are 9.39µm and 45.11µm, respectively. In initial condition were 4.3µm and 25.57µm. The factors that contribute to this region to present high values of roughness are the same acting in C_2.

The micrographs of three points of the mask are shown in Figure 12, the images are from the middle of each positions shown in the schematic representation. In position 2 is possible to observe the same formation of position 1, which indicates that the tempering of the bainite occurred in all regions of the mask. The tempering, resulting from a long time in contact with the forging billets at temperatures above 700ºC. It can be observed that the microstructural morphology is characterized by the change of structure to equiaxial perlite.

The tempering of bainite was reflected in the microhardness profile (Figure 13), where the reduction in values is observed in the regions of center, r_1, mask wall, r_2 and flash gutter with values between 215HV and 285HV. It is possible to observe the reduction in the microhardness profile values in all regions that were in contact with the part during forging cycles. The flange region shows a gradual increase in the microhardness values, approaching the initial hardness, the average microhardness is 407.8HV.

Figure 14 shows micrography obtained by SEM of the r_1 n r_2 of the side of the mask that was in contact with billet during the forging, that is, those that were in contact with the forged part. It is possible to observe the progressive degradation, that is, the removal of material by abrasion of the surface occurred, displacement marks and micro cracks. This characteristic is accentuated in r_1. The cracks propagation indicates that wear acting of surface is accentuated by plastic deformation.

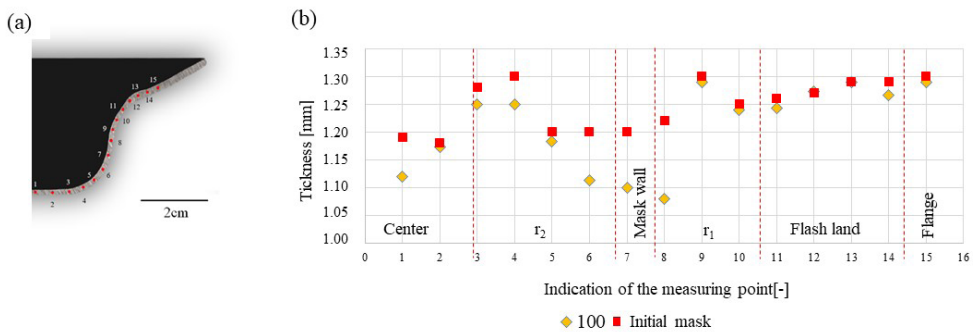

Figure 11. Variation in the thickness of the axial masks in different regions: (a) Indication of the measurement points on the cross-section mask and (b) Mask thickness values in the initial condition and after 100 forging cycles.

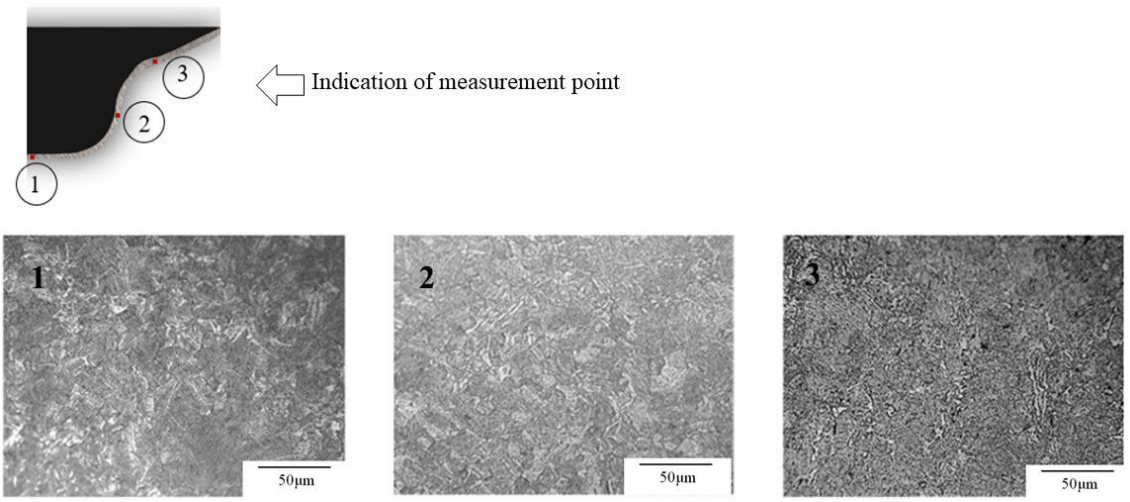

Figure 12. Optical micrographs of the transverse section of the axial mask after 100 forging cycles, with positions indicated in the schematic representation: (1) Center of the sample, (2) After radius 2 and (3) After radius 2.

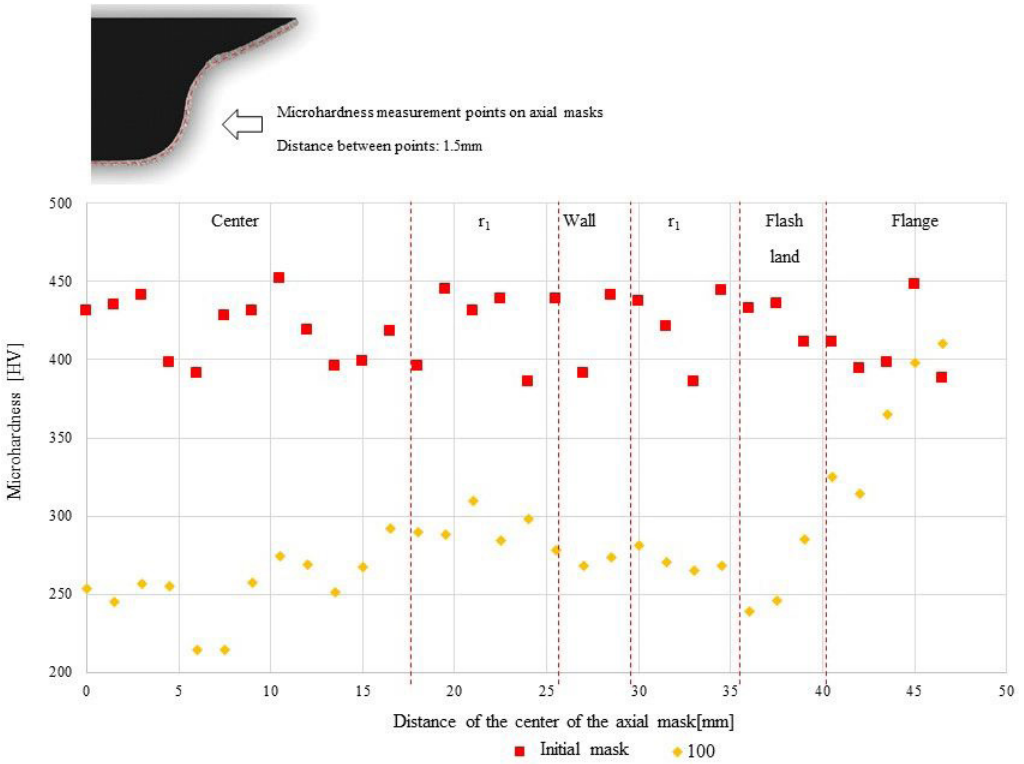

Figure 13. Vickers microhardness profile of the axial masks.

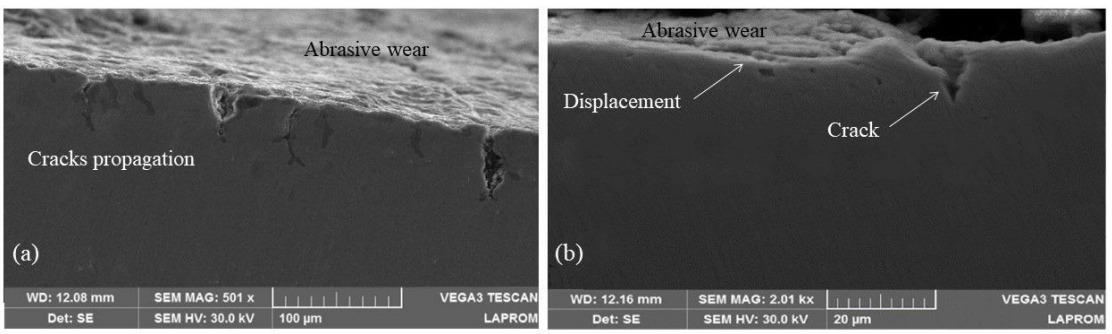

Figure 14. Micrographs obtained by electron microscopy (SEM) of the surface of the r_1 (a) and r_2 (b) of the axial mask after the forging cycles.

4. Conclusion

During hot forging processes the dies are exposed to degradation mechanisms that progress until the tools needed to be changed. This study aimed to analyze the applicability of masks as surface protection in forging in open and closed die, allowing to conclude that:

- In the flat mask, the region 1 remains in contact with the billet throughout the forging cycle and presents the greatest reductions in thickness and hardness and increase in roughness occur (Ra, Rz).
- The reduction of hardness is progressive in the axial mask, being close to the initial in the region of the flange and reducing to the central region. The roughness (Ra, Rz) is greatest in the side which remains in contact with die.
- The reduction hardness in both masks is attributed to the formation of bainite in the initial masks and the tempering of the bainite after the 100 forging cycle.
- The predominant wear mechanisms in the masks surfaces were abrasive wear and plastic deformation.
- Considering the conditions of the forging processes to which the flat and axial masks were exposed, both not presented any failure that would render them unusable until the 100 forging cycle.

5. Acknowledgments

The authors thank IBF–RWTH Aachen University (Germany) for the technical partnership in the project BRAGECRIM; CNPq (National Council for Scientific and Technological Development) and Capes (Coordination for the Improvement of Higher Education Personnel) for financial support; and the Laboratório de Processamento Mineral (LAPROM) for technical support.

6. References

1. EUROFORGE [homepage on the Internet]. 2019 [cited 2023 Apr 29]. Available from: www.euroforge.org.
2. Pereira MH, Souza RM, Souza TSG. Desgaste do punção de forjamento a quente – mecanismos de desgaste. In: XIV Simpósio Internacional de Engenharia Automotiva; 2016; São Paulo, Brasil. Proceedings. São Paulo: Blucher; 2016. p. 464-80.
3. OICA - Organisation Internationale des Constructeurs d'Automobiles. International Organization of Motor Vehicle Manufacturers [homepage on the Internet]. 2020 [cited 2023 Apr 29]. Available from: www.oica.net/
4. Hawryluka M, Gronostajkia Z, Kaszubaa M, Polaka S, Widomskia P, Smolikb J, et al. Analysis of the wear of forging tools surface layer after hybrid surface treatment. Int J Mach Tools Manuf. 2017;114:60-71. http://dx.doi.org/10.1016/j.ijmachtools.2016.12.010.
5. Behrens BA, Rubner S, Demir M. Conductive heating system for hot sheet metal forming. In: 1st International Conference on Hot Sheet Metal Forming of High-Performance Steel; Kassel, Germany. Proceedings. Bad Harzburg: GRIPS Media; 2008. p. 63-68.
6. Santaella ML. Thermo-mechanical fatigue of hot forging tool predicition, analys and aptimization methods through six-sigma. Aachen, Germany: Fakultät für Georessourcen und Materialtechnik - IWT Aachen; 2013.
7. Altan T, Ngaile G, Shen G. Cold and hot forging: fundamental and application. Materials Park OH: ASM International, 2004.
8. Hawryluk M. Review of selected methods of increasing the life of forging tools in hot die forging processes. Arch Civ Mech Eng. 2016;16(4):845-66. http://dx.doi.org/10.1016/j.acme.2016.06.001.
9. Rosenstock D, Segebade ET, Hirt G. First experimental and numerical study on the use of sheet metal die covers for wear protection in closed-die forging. Key Eng Mater. 2015;651:266-71.
10. Yu Y, Zottis J, Wolfgarten M, Hirt G. Investigation of applying protective sheet metal die covers for hot forging dies on a cross-forging geometry. Int J Adv Manuf Technol. 2019;102(1-4):999-1007. http://dx.doi.org/10.1007/s00170-018-03250-4.
11. Gronostajski Z, Kaszuba M, Hawryluk M, Zwierzchowski M. A review of the degradation mechanisms of the hot forging tools. Arch Civ Mech Eng. 2014;14(4):528-39. http://dx.doi.org/10.1016/j.acme.2014.07.002.
12. Karbasian H, Tekkaya A. A review on hot stamping. J Mater Process Technol. 2010;210(15):2103-2118. http://dx.doi.org/10.1016/j.jmatprotec.2010.07.019.
13. George R, Bardelcik A, Worswick MJ. Hot forming of boron steels using heated and cooled tooling for tailored. J Mater Process Technol. 2012;212(11):2386-99. http://dx.doi.org/10.1016/j.jmatprotec.2012.06.028.
14. Batalha ME. Estudo da estampabilidade a quente de aço ao boro em conformação com redução comparada [dissertation]. Campinas, Brasil: Faculdade de Engenharia Mecânica, UNICAMP; 2015.
15. Rodrigues J, Martins P. (2010). Tecnologia Mecânica. Volume II - Aplicações Industriais. Lisboa, Portugal: Dinternal.
16. ASM International. Metallography and Microstructure. 9th ed. ASM International: Materials Park, OH, USA; 2004. (Vol. 9).